

On the measurement of two-photon single-mode coupling efficiency in parametric down-conversion photon sources

This article has been downloaded from IOPscience. Please scroll down to see the full text article.

2004 New J. Phys. 6 87

(<http://iopscience.iop.org/1367-2630/6/1/087>)

View [the table of contents for this issue](#), or go to the [journal homepage](#) for more

Download details:

IP Address: 38.107.179.214

The article was downloaded on 20/02/2012 at 16:11

Please note that [terms and conditions apply](#).

On the measurement of two-photon single-mode coupling efficiency in parametric downconversion photon sources

S Castelletto¹, I P Degiovanni¹, A Migdall² and M Ware²

¹ Istituto Elettrotecnico Nazionale G Ferraris, Strada delle Cacce 91-10135, Torino, Italy

² Optical Technology Division, National Institute of Standards and Technology, Gaithersburg, MD 20899-8441, USA

E-mail: castelle@ien.it and amigdall@nist.gov

New Journal of Physics **6** (2004) 87

Received 5 February 2004

Published 29 July 2004

Online at <http://www.njp.org/>

doi:10.1088/1367-2630/6/1/087

Abstract. Photon-based quantum information schemes have increased the need for light sources that produce individual photons, with many such schemes relying on optical parametric downconversion (PDC). Practical realizations of this technology require that the PDC light be collected into a single spatial mode defined by an optical fibre. We present two possible models describing single-mode fibres coupling to PDC light fields in a non-collinear configuration, that lead to two different results. These approaches include factors like crystal length, and walk-off, non-collinear phase-matching, and transverse pump field distribution. We propose an experimental test to distinguish between the two. The goal is to help clarify open issues, such as how to extend the theory beyond the simplest experimental arrangements, and more importantly, to suggest a way to improve the collection efficiency.

Contents

1. Introduction	2
2. Definition of PDC field- and intensity-based collection efficiencies	3
2.1. PDC single-mode field-based collection efficiency	4
2.2. PDC single-mode intensity-based collection efficiency	5
3. Calculation of the field-based collection efficiency	6
4. Calculation of the single-mode intensity-based collection efficiency	9
5. Discussion of results	11
6. Conclusions	15
Acknowledgments	15
References	15

1. Introduction

The advent of photon-based quantum cryptography, communication, and computation schemes [1]–[10] has increased the need for light sources that produce individual photons [11]. An ideal single-photon source would produce completely characterized single photons on demand. Because all of the currently available sources fall significantly short of this ideal (that is they do not produce photons 100% of the time and/or they do not produce only single photons), much effort has been focused on creating improved approximations of single-photon-on-demand sources (SPOD) [12]–[19]. Some of these schemes [17, 19] rely on optical parametric downconversion (PDC), because it produces photons two at a time, allowing one photon to herald the existence of the other. In a previous work, we proposed one such scheme where a multiplexed PDC array is used to make an improved SPOD source with increased probability of single-photon emission, while suppressing the probability of multi-photon generation [19]. Most PDC-based schemes (including ours) require that the PDC output be collected into a single spatial mode defined by an optical fibre. For these PDC schemes to reliably produce single photons, it is essential that the optical collection system efficiently gathers and detects the herald photon, and with minimal loss, sends its partner to the output of the system. In addition to SPOD applications, it is also important to understand collection efficiency for other applications such as PDC-based metrological applications, which are very sensitive to collection efficiency [20].

Various theoretical models have been developed to predict how the collection efficiency of PDC light in a ‘two-photon single-mode’ can be improved [21]–[24], and in some cases these models have been used to improve coupling efficiency. In particular, it has been shown that the size of the pump beam focus affects the shape of the PDC output [21] and hence the coupling efficiency of the PDC light into a given spatial mode. In addition, a more detailed work [23] recently showed how increasing the crystal length and walk-off reduces the coupling efficiency for a pulsed broadband pump. However, in these works, the attempts to increase the single-mode fibre coupling efficiency were limited to a tightly focused pump beam and a thin crystal, which reduces the overall source brightness. This last restriction is forced on

the calculations because the approximations used for the phase-mismatch function in terms of longitudinal wavevector mismatch are not valid in the long-crystal case. Moreover, these works deal only with either type I or II phase-matching conditions exclusively; they do not include the non-collinearity and/or walk-off of the emitted photons and the pump beam. The work done to date does however give some partial guidance for increasing coupling efficiency in certain experimental situations. For instance, the most practical results to date generally show that the collection efficiency for long crystals is optimized for properly matched large pump and collection waists. However the maximum efficiency is limited by walk-off in type II [23] phase-matching and by excessive crystal length in type I phase-matching [24]. Furthermore, the approximations done in the previous theory limited the validity of the results to a narrow range of crystal lengths and collection/pump waists.

A more general approach to the problem is needed to clarify open issues such as those mentioned above (i.e. overcoming the calculational limits and extending the theory), and to determine how we can best test the collection efficiency model. Here, we present one model to describe the coupling of the PDC source into single spatial modes. This method uses a field-based model to describe the coupling of the PDC field with single-mode fibre defined fields, as has been partially presented in other works along with some suggestive supporting data [23, 24]. We also consider an alternate intensity-based model, where an intensity projector operator represents the effect of a spatial filtering, as suggested in [21, 25]. We calculate the collection efficiencies using both methods for both type I and II PDC output into two single-modes defined by optical fibres, accounting for effects due to the crystal length, walk-off of extraordinary fields, non-collinear phase-matching, and pump transverse field distribution. We then analytically evaluate both efficiencies assuming negligible second-order terms in the transverse component of the wavevectors. The intensity-based approach exhibits counter-intuitive results, even in the thin crystal limit and may be more suitable for multi-mode collection. We propose an experimental test to distinguish between the two.

The work is organized as follows, in section 2 we define the field- and intensity-based collection efficiencies for a PDC field. In sections 3 and 4, we explicitly calculate the two efficiencies in terms of the parameters of the physical systems. In section 5, we compare the predictions of the two models.

2. Definition of PDC field- and intensity-based collection efficiencies

To determine the collection efficiency of the parametric downconversion output into two single spatial modes (defined in our setup by single-mode optical fibres and lenses as shown in figure 1), we use two very different approaches. In the first, we calculate the overlap of the PDC field with the field modes selected by the fibres and indirectly evaluate coincidences and singles. In the second, we calculate the PDC wave function over the spatial distribution of intensities as defined by single-mode fibres directly providing coincidences and associated singles counts. The main difference between the two approaches relates to the fibre-mode selection and associated detection process. The first assumes that the fibre plus the detector is a system able to distinguish single-mode fields, and the calculation is therefore performed in terms of fields rather than intensities. The second assumes that the fibres select the mode and the detectors measure the associated intensity.

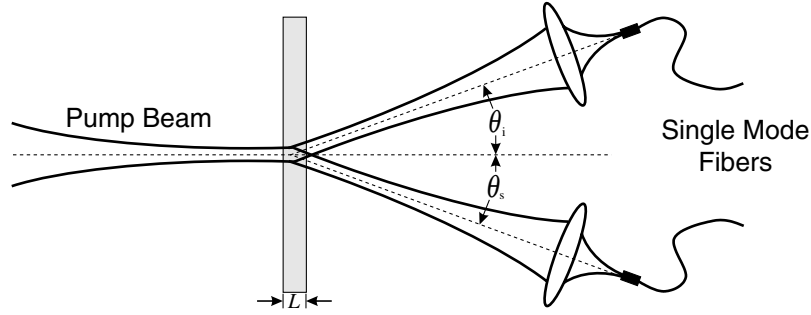


Figure 1. PDC is generated in non-linear crystals of length L , by a pump beam with a Gaussian profile, and is collected into single-mode optical fibres as imaged by lenses.

2.1. PDC single-mode field-based collection efficiency

In the field-based approach, the first step is to calculate the two-photon PDC field [26] given by

$$A_{12}(\mathbf{r}_1, \mathbf{r}_2, t_1, t_2) = \langle 0 | \hat{E}_s^{(+)}(\mathbf{r}_1, t_1) \hat{E}_i^{(+)}(\mathbf{r}_2, t_2) | \psi \rangle, \quad (1)$$

where $|0\rangle$ is the vacuum state, and $|\psi\rangle$ is the two-photon wavefunction, written as

$$|\psi\rangle = \int d^3r_1 d^3r_2 dt_1 dt_2 \tilde{\Phi}(\mathbf{r}_1, \mathbf{r}_2, t_1, t_2) |1_{\mathbf{r}_2, t_2}\rangle |1_{\mathbf{r}_1, t_1}\rangle, \quad (2)$$

with $\mathbf{r}_{1,2}$ describing the positions of the two-photon at the instant $t_{1,2}$ and $\tilde{\Phi}(\mathbf{r}_1, \mathbf{r}_2, t_1, t_2)$ is the phase-matching function. The subscripts s , i and p indicate the signal, idler and pump, respectively. The fields

$$\hat{E}_{s,i}^{(+)}(\mathbf{r}_{1,2}, t_{1,2}) = N_E \int d^3k_{s,i} d\omega_{s,i} \hat{a}_{\mathbf{k}_{s,i}, \omega_{s,i}} \exp[i(\mathbf{k}_{s,i} \cdot \mathbf{r}_{1,2} - \omega_{s,i} t_{1,2})] \quad (3)$$

are the positive-frequency portions of the electric field operator evaluated at positions \mathbf{r}_j , and times t_j . N_E is a normalization factor and $\hat{a}_{\mathbf{k}_{s,i}, \omega_{s,i}}$ is the photon annihilation operator. To determine the collection efficiency, we write A_{12} as a coherent superposition of guided modes, $\varphi_{lm}^*(x, y)$, in the fibre as suggested in [23]

$$A_{12}(\mathbf{r}_1, \mathbf{r}_2, t_1, t_2) = \sum_{l'm', lm} A_{12}^{l'm', lm}(z_1, z_2, t_1, t_2) \varphi_{l'm'}^*(x_1, y_1) \varphi_{lm}^*(x_2, y_2). \quad (4)$$

The field-based collection efficiency can then be written as

$$\chi_{12} = \frac{C_{12}}{\sqrt{C_1 C_2}}, \quad (5)$$

where \mathcal{C}_{12} is the fractional power [27] of the biphoton field coupled to the two single-mode fibres; i.e. the overlap between the PDC field with both collection modes. Likewise \mathcal{C}_1 , and \mathcal{C}_2 are the fractional powers of the biphoton field coupled to each single-mode fibre, defined by the overlap between the biphoton field and each collection mode:

$$\begin{aligned}\mathcal{C}_{12} &= \int dz_1 dt_1 dz_2 dt_2 \left| \int dx_1 dy_1 dx_2 dy_2 A_{12}(\mathbf{r}_1, t_1, \mathbf{r}_2, t_2) \varphi_{l'm'}(x_1, y_1) \varphi_{lm}(x_2, y_2) \right|^2, \\ \mathcal{C}_1 &= \int dz_1 dt_1 dt_2 d^3 r_2 \left| \int dx_1 dy_1 A_{12}(\mathbf{r}_1, t_1, \mathbf{r}_2, t_2) \varphi_{l'm'}(x_1, y_1) \right|^2, \\ \mathcal{C}_2 &= \int dz_2 dt_2 dt_1 d^3 r_1 \left| \int dx_2 dy_2 A_{12}(\mathbf{r}_1, t_1, \mathbf{r}_2, t_2) \varphi_{l'm'}(x_2, y_2) \right|^2.\end{aligned}\quad (6)$$

This approach for obtaining the efficiency χ_{12} is similar to classical photonics theory. However, the same result can be obtained by a quantum mechanical approach with projectors given by

$$\widehat{P}_{l,m}^{(j)} = |1_{lm}^{(j)}\rangle \langle 1_{lm}^{(j)}|, \quad (7)$$

where

$$|1_{lm}^{(j)}\rangle = \int d^2 \rho_j \varphi_{lm}(\rho_j) |1_{\rho_j}\rangle \quad (8)$$

with $j = 1, 2$. The coincidences can then be calculated by projecting the wavefunction over two single-mode fibres:

$$\mathcal{C}_{12} \propto \text{Tr}[|\psi\rangle \langle \psi| \widehat{P}_{lm}^{(1)} \widehat{P}_{l'm'}^{(2)}] \quad (9)$$

and the singles are given by

$$\mathcal{C}_j \propto \text{Tr}[|\psi\rangle \langle \psi| \widehat{P}_{lm}^{(j)}]. \quad (10)$$

2.2. PDC single-mode intensity-based collection efficiency

In the intensity-based approach, the projectors representing the spatial distribution of a single-mode fibre are given by

$$\widehat{P}_j = \int d^3 r_j dt_j \mathcal{I}_j(\mathbf{r}_j, t_j) |1_{\mathbf{r}_j, t_j}\rangle \langle 1_{\mathbf{r}_j, t_j}|, \quad (11)$$

with $j = 1, 2$. $\mathcal{I}_j(\mathbf{r}_j, t_j)$ are the intensity profiles of the single-mode spatial distribution of the fields. This approach is similar to the approach of [25], which considers conditionally prepared

photon states. The coincidences calculated by projecting the wavefunction over two single-mode fibres are then

$$C_{12} = \text{Tr}[|\psi\rangle\langle\psi|\widehat{P}_1\widehat{P}_2] = \int d^3r_1 d^3r_2 dt_1 dt_2 |\widetilde{\Phi}(\mathbf{r}_1, \mathbf{r}_2, t_1, t_2)|^2 \mathcal{I}_1(\mathbf{r}_1, t_1) \mathcal{I}_2(\mathbf{r}_2, t_2), \quad (12)$$

and the singles are given by

$$S_j = \text{Tr}[|\psi\rangle\langle\psi|\widehat{P}_j] = \int d^3r_1 d^3r_2 dt_1 dt_2 |\widetilde{\Phi}(\mathbf{r}_1, \mathbf{r}_2, t_1, t_2)|^2 \mathcal{I}_j(\mathbf{r}_j, t_j). \quad (13)$$

The single-mode intensity-based collection efficiency is then defined by

$$\eta_{12} = \frac{C_{12}}{\sqrt{S_1 S_2}}. \quad (14)$$

3. Calculation of the field-based collection efficiency

The two-photon state at the output surface of a PDC crystal oriented with its face perpendicular to the z -axis is given by [26]

$$|\psi\rangle = \int d^3k_s d\omega_s d^3k_i d\omega_i \Phi(\mathbf{k}_s, \mathbf{k}_i, \omega_i, \omega_s) |1_{\mathbf{k}_s, \omega_s}\rangle |1_{\mathbf{k}_i, \omega_i}\rangle, \quad (15)$$

where $\Phi(\mathbf{k}_s, \mathbf{k}_i, \omega_i, \omega_s)$ is given by

$$\begin{aligned} \Phi(\mathbf{k}_s, \mathbf{k}_i, \omega_i, \omega_s) = & N \int d^3k_p d\omega_p \int_S dx dy \int_{-L}^0 dz \widetilde{E}_p(\mathbf{q}_p) e^{i(\Delta k_x x + \Delta k_y y + \Delta k_z z)} \\ & \times \delta(\omega_s + \omega_i - \omega_p) \delta(\omega_p - \Omega_p) \\ & \times \delta \left[\mathbf{k}_p \cdot \mathbf{p}_z - \sqrt{\left(\frac{n(\Omega_p) \Omega_p}{c} \right)^2 - \mathbf{q}_p^2} \right] \\ & \times \delta \left[\mathbf{k}_s \cdot \mathbf{s}_z - \sqrt{\left(\frac{n(\omega_s) \omega_s}{c} \right)^2 - \mathbf{q}_s^2} \right] \\ & \times \delta \left[\mathbf{k}_i \cdot \mathbf{i}_z - \sqrt{\left(\frac{n(\omega_i) \omega_i}{c} \right)^2 - \mathbf{q}_i^2} \right], \end{aligned} \quad (16)$$

where S is the cross sectional area of the crystal illuminated by the pump, N the normalization factor, and L the length of the crystal. The subscripts s , i and p indicate the signal, idler and pump. We denote the crystal axes in the lab frame by \mathbf{c}_x , \mathbf{c}_y , \mathbf{c}_z , with the pump beam propagating along \mathbf{c}_z . Because the signal and idler wavevectors do not generally point along the crystal axes,

we identify the pump, signal, and idler \mathbf{k} -vector directions as \mathbf{p}_z , \mathbf{s}_z , \mathbf{i}_z , and their transverse components as $\mathbf{p}_{x,y}$, $\mathbf{s}_{x,y}$, $\mathbf{i}_{x,y}$. Using the above notation, we evaluate $\Delta k_{x,y,z}$. Given that $\Delta k_{x,y,z} = (\mathbf{k}_p - \mathbf{k}_s - \mathbf{k}_i) \cdot \mathbf{c}_{x,y,z}$, we write $\Delta k_{x,y,z}$ in terms of the pump, signal, and idler \mathbf{k} -vectors. The longitudinal component of the pump \mathbf{k} -vector is

$$\mathbf{k}_p \cdot \mathbf{p}_z = \sqrt{\left(\frac{n(\Omega_p)\Omega_p}{c}\right)^2 - \mathbf{q}_p^2}, \quad (17)$$

where \mathbf{q}_p is the transverse component of the pump \mathbf{k} -vector and c is the speed of light. Analogous expressions give the signal and idler longitudinal components.

We now make some approximations to evaluate $\Delta k_{x,y,z}$. First, we assume that the pump, signal and idler have narrow transverse angular distributions, so we can adopt the paraxial approximation. We also rewrite the longitudinal \mathbf{k} -vector components by expanding the index of refraction $n_{p,s,i}(\omega_{p,s,i}, \phi)$ around the central frequencies ($\Omega_{s,i}$), and around the phase-matching angle ϕ_o . This last approximation holds only in cases where the considered field is an extraordinary wave (this of course depends on the type of phase-matching adopted, either type I or II). In all cases, we limit our calculation to the first perturbative order. We also assume small non-collinearity and small walk-off angles. When these two approximations hold, we can expand the sine and cosine terms, limited to first order. Finally, we write the overall $\Delta k_{x,y,z}$ terms as

$$\begin{aligned} \Delta k_x &= \mathbf{q}_p \cdot \mathbf{p}_x - \mathbf{q}_s \cdot \mathbf{s}_x - \mathbf{q}_i \cdot \mathbf{i}_x, \\ \Delta k_y &= \mathbf{q}_p \cdot \mathbf{p}_y - \mathbf{q}_s \cdot \mathbf{s}_y - \mathbf{q}_i \cdot \mathbf{i}_y - \theta_i K_i - \theta_s K_s, \\ \Delta k_z &= Dv + (\mathcal{N}_p - \mathcal{N}_s) \frac{\mathbf{q}_p \cdot \mathbf{p}_y}{K_p} + \theta_s \mathbf{q}_s \cdot \mathbf{s}_y - \theta_i \mathbf{q}_i \cdot \mathbf{i}_y, \end{aligned} \quad (18)$$

where $\theta_{i,s}$ are the emission angles of the idler and signal photons, $K_{i,s,p} = n_{i,s,p}(\Omega_{i,s,p}, \phi) \Omega_{i,s,p}/c$ describe the directions of the central intensities of the wavevectors. The terms, $\mathcal{N}_p = \frac{\Omega_p}{c} \frac{dn_p(\Omega_p, \phi)}{d\phi} |_{\phi_o}$ and $\mathcal{N}_s = \frac{\Omega_s}{c} \frac{dn_s(\Omega_s, \phi)}{d\phi} |_{\phi_o}$ account for the effects on the refractive indexes of the pump and the signal due to the pump angular spread, which is responsible for a small deviation from the phase-matching angle ϕ_o . The other terms are defined as $D = -\frac{dn_i(\omega_i)\omega_i/c}{d\omega_i} |_{\Omega_i} + \frac{dn_s(\omega_s, \phi)\omega_s/c}{d\omega_s} |_{\Omega_s}$ and $v = \omega_s - \Omega_s = \Omega_i - \omega_i$. Note that $\mathcal{N}_s = 0$ for type I phase-matching. The first term in the expression for Δk_z accounts for the differential phase velocity between the signal and idler photons in the crystal, which is zero for type I degenerate; the second terms are responsible for the pump and signal walk-offs, respectively. (The signal and idler walkoff is generally zero for type I.) These terms account also for the pump transverse distribution as an angular spread around a principal direction, and the last two terms are associated with the non-collinear emission of the photons. We note that in the type I degenerate case, these last two terms cancel out.

The pump beam transverse field distribution is defined via the Fourier transform

$$E_p(\boldsymbol{\rho}) = \frac{1}{2\pi} \int d^2 q_p \tilde{E}_p(\mathbf{q}_p) e^{i\mathbf{q}_p \cdot \boldsymbol{\rho}}. \quad (19)$$

We take this transverse distribution to be Gaussian with a waist of w_p at the crystal, and assume that the transverse crystal size is large relative to the pump beam, so we can take the cross section, S , to be infinite. Moreover, we assume that the pump beam has a narrow angular spectrum

(transverse wavevector distribution) and that the signal and idler are observed only at points close to their central directions. The central frequencies are $\Omega_{s,i}$. We also assume that the pump propagates with negligible diffraction inside the crystal, so that $E_p(\rho)$ is independent of z . With these approximations, we calculate the valid ranges of w_p , L and w_o , the width of collection fibre mode as imaged at the crystal. In particular, $L \ll K_p w_p^2/2$ to have negligible diffraction of the pump in the crystal. We can neglect second-order terms in the transverse wavevector component in (18) when $w_{o,p} \gg (K_{s,i} \theta_{s,i})^{-1}$.

Using these approximations we rewrite (15) as

$$|\psi\rangle = N \int_{-L}^0 dz \int d^2 q_s d^2 q_i d^2 q_p d\nu \tilde{E}_p(\mathbf{q}_p) e^{i\Delta k_z z} \delta(\Delta k_x) \delta(\Delta k_y) |1_{\mathbf{k}_s, \omega_s}\rangle |1_{\mathbf{k}_i, \omega_i}\rangle. \quad (20)$$

To evaluate C_{12} and $S_{1,2}$, we rewrite the state $|\psi\rangle$ in terms of $|1_{\mathbf{r}_1, t_1}\rangle |1_{\mathbf{r}_2, t_2}\rangle$, using

$$|1_{\mathbf{k}_s, \omega_s}\rangle = \frac{1}{(2\pi)^2} \int d^3 r_1 dt_1 e^{i(\mathbf{k}_s \cdot \mathbf{r}_1 - \omega_s t_1)} |1_{\mathbf{r}_1, t_1}\rangle \quad (21)$$

and

$$|1_{\mathbf{k}_i, \omega_i}\rangle = \frac{1}{(2\pi)^2} \int d^3 r_2 dt_2 e^{i(\mathbf{k}_i \cdot \mathbf{r}_2 - \omega_i t_2)} |1_{\mathbf{r}_2, t_2}\rangle. \quad (22)$$

Thus the $\Phi(\mathbf{k}_s, \mathbf{k}_i, \omega_i, \omega_s)$ in (16) becomes, in the new basis, its Fourier transform $\tilde{\Phi}(\mathbf{r}_1, \mathbf{r}_2, t_1, t_2)$, as indicated formally in (2) and calculated at the output surface of the crystal ($z_{1,2} = 0$). By performing the Fourier transforms and leaving the z integration for last, we obtain

$$\begin{aligned} \tilde{\Phi}(\mathbf{r}_1, \mathbf{r}_2, t_1, t_2) &= N_1 \exp\left[\frac{-i(K_i \theta_i^2 + K_s \theta_s \theta_i \tau)}{D}\right] \exp\left[\frac{-(\mathcal{N}_p - \mathcal{N}_s)^2 \tau^2}{D^2 w_p^2 K_p}\right] \\ &\times \exp\left[\frac{2(\mathcal{N}_p - \mathcal{N}_s) \tau (y_1 + \frac{\theta_i \tau}{D})}{D w_p^2 K_p}\right] \exp\left[-\frac{x_1^2 + (y_1 + \frac{\theta_i \tau}{D})^2}{w_p^2}\right] \Pi_{DL}(\tau) \\ &\times \delta(x_1 - x_2) \delta\left(y_1 - y_2 + \frac{(\theta_i + \theta_s) \tau}{D}\right) \delta(z_1) \delta(z_2), \end{aligned} \quad (23)$$

where $\tau = t_1 - t_2$ and $\Pi_{DL}(\tau) = 1$ for $0 \leq \tau \leq DL$ and 0 elsewhere. To guarantee that the biphoton state is properly normalized, the factor N_1 is determined from the condition $\int d^3 r_1 d^3 r_2 dt_1 dt_2 |\tilde{\Phi}(\mathbf{r}_1, \mathbf{r}_2, t_1, t_2)|^2 = 1$, giving $N_1 = w_p / (4\pi^2 \sqrt{DL})$. To calculate the field-based collection efficiency, we assume the guided mode is a Gaussian field at the crystal output surface, defined by

$$\varphi_{10}^*(x_j, y_j) = \sqrt{\frac{2}{\pi}} \frac{1}{w_o} \exp\left[-\frac{(x_j^2 + y_j^2)}{w_o^2}\right]. \quad (24)$$

The imaging optic is arranged to place the collection beam waist, w_o at the crystal. The intensity of the collection modes are normalized by setting $\int [\varphi_{10}^*]^2 dx dy = 1$, which yields the coefficient

in (24). The biphoton field is calculated using (1), (3) and (23), and the operator

$$\hat{a}_{\mathbf{k}_{s,i},\omega_{s,i}} = \frac{1}{(2\pi)^2} \int d^3r_{1,2} dt_{1,2} \hat{a}_{\mathbf{r}_{1,2},t_{1,2}} \exp^{-i\mathbf{k}_{s,i} \cdot \mathbf{r}_{1,2} + \omega_{s,i} t_{1,2}} \quad (25)$$

to obtain

$$A_{12}(\mathbf{r}_1, \mathbf{r}_2, t_1, t_2) \propto N_E^2 \tilde{\Phi}(\mathbf{r}_1, \mathbf{r}_2, t_1, t_2). \quad (26)$$

The single-mode field-based collection efficiency is then given by

$$\chi_{12} = \mathcal{F} \frac{4w_o w_p^2 \sqrt{(w_o^2 + w_p^2)(-\mathcal{N}_p + \mathcal{N}_s + K_p \theta_i)(\mathcal{N}_p - \mathcal{N}_s + K_p \theta_s)}}{\sqrt{(w_o^2 + 2w_p^2)^3 B}}, \quad (27)$$

with

$$\mathcal{F} = \frac{\text{Erf} \left[\frac{L\sqrt{B}}{K_p w_o \sqrt{w_o^2/2 + w_p^2}} \right]}{\sqrt{\text{Erf} \left[\sqrt{2}L \frac{(-\mathcal{N}_p + \mathcal{N}_s + K_p \theta_i)}{K_p \sqrt{w_o^2 + w_p^2}} \right] \text{Erf} \left[\sqrt{2}L \frac{(\mathcal{N}_p - \mathcal{N}_s + K_p \theta_s)}{K_p \sqrt{w_o^2 + w_p^2}} \right]}} \quad (28)$$

and $B = (2\mathcal{N}_p^2 + 2\mathcal{N}_s^2 - 2\mathcal{N}_p(2\mathcal{N}_s + K_p(\theta_i - \theta_s)) + 2K_p\mathcal{N}_s(\theta_i - \theta_s) + K_p^2(\gamma_s^2 + \theta_i^2 + \theta_s^2))w_o^2 + K_p^2(\theta_i + \theta_s)^2 w_p^2$. In the thin crystal limit this reduces to

$$\chi_{12} = \frac{4w_p^2(w_o^2 + w_p^2)}{(w_o^2 + 2w_p^2)^2} \quad (29)$$

as first calculated in [23, 24]. In this approach the fibres act to project the photons' state onto a specific propagation mode both in amplitude and phase, as indicated in (7) and (8). The spatial coherence of the single guided modes in the signal and idler arms should ultimately match the overall spatial coherence of the two-photon states.

4. Calculation of the single-mode intensity-based collection efficiency

To calculate the single-mode intensity-based collection efficiency, we assume the projectors \hat{P}_j , representing the fibre modes propagated back to the output surface of the crystal, are completely determined by the functions

$$\mathcal{I}_j(\mathbf{r}_j) = \exp \left[-\frac{2(x_j^2 + y_j^2)}{w_j^2} \right] \delta(z_j). \quad (30)$$

(Note that in this approach, the intensity projection operator has a maximum of 1 because of its probabilistic nature.) We assume the conditions detailed following (19) are valid and also that

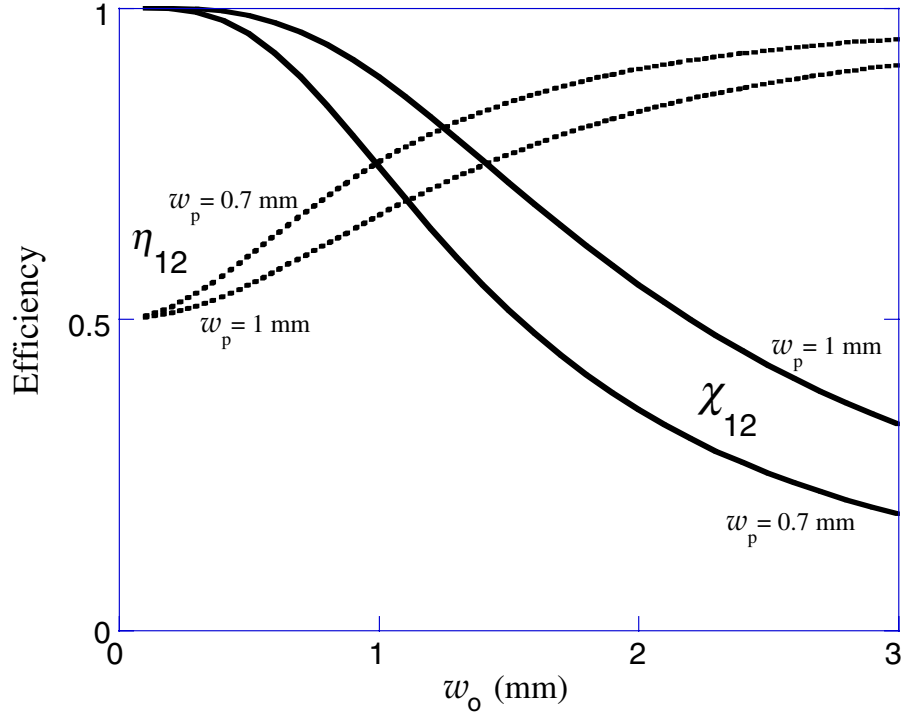


Figure 2. Field-based collection efficiency (—) and intensity-based collection efficiency (\cdots) in the thin crystal limit versus w_o , for fixed values of w_p .

$w_s = w_i = w_o$, and then calculate the single-mode intensity-based collection efficiency:

$$\eta_{12} = \mathcal{F} \frac{w_o \sqrt{(w_o^2 + w_p^2)(-\mathcal{N}_p + \mathcal{N}_s + K_p \theta_i)(\mathcal{N}_p - \mathcal{N}_s + K_p \theta_s)}}{\sqrt{(w_o^2 + 2w_p^2)B}}. \quad (31)$$

In the thin crystal limit, η_{12} becomes

$$\eta_{12} = \frac{w_o^2 + w_p^2}{(w_o^2 + 2w_p^2)}. \quad (32)$$

Note that there are several approximations other than $L \rightarrow 0$ that lead to (32). For example, the assumptions following (19) preclude the case of an arbitrarily small pump waist at the crystal. The collection-mode waist is also restricted to modes that can be created by finite lenses that image fibres at a finite distance from the crystal.

In the intensity-based approach presented in this section, the collection mode can be thought of as spatially filtering the multi-mode input light. Thus, it is likely to be better suited for modelling multi-mode fibre collection. As the next section demonstrates, the predictions made by this model yield results different from the field-based model. The intensity-based model predicts that, for a fixed pump waist, the maximum collection efficiency is obtained when the fibre-defined collection

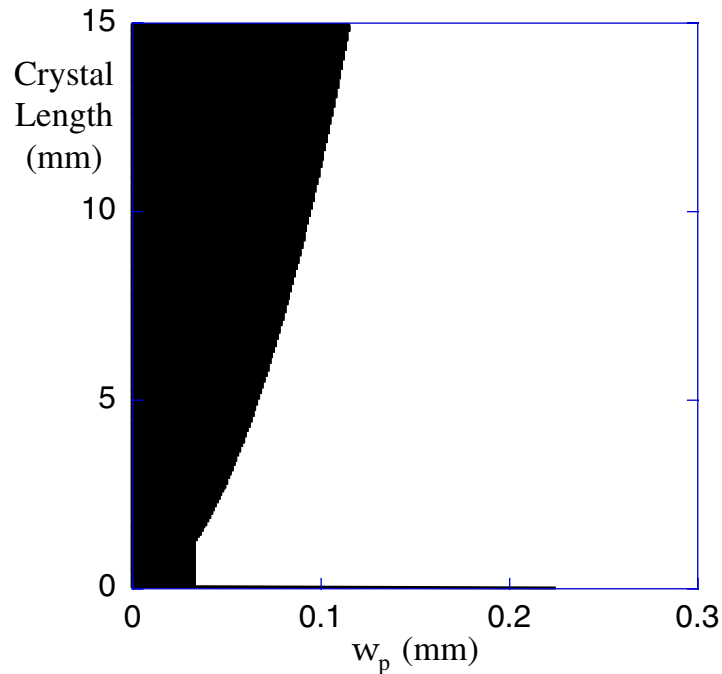


Figure 3. Plot of the range of values for L and w_p to guarantee the validity of the final formula (white region). Calculations are in the conditions of $w_o \geq w_p$ (a trivial convenient experimental choice) and non-collinear phase-matching for the angles and frequencies given in section 5.

mode (at the crystal) is large, i.e. all the pumped crystal volume is in a region of unit collection efficiency of the fibre/spatial filter system. With the field-based approach, the optics setup of figure (1), can be envisioned in an unfolded geometric arrangement [28] where one of the fibres acts as a single-mode source propagating back through a spatial filter (in this case the pumped crystal volume) to the other fibre. The maximum collection is achieved with a large pump waist, with respect to the collection beam waist at the crystal. If the pump waist is smaller than the fibre-defined collection beam waist, the collection efficiency is reduced. It is likely that the field-based approach gives the best answers for a single-mode fibre. However, moving to multi-mode fibres, the result should approach the intensity-based model, i.e. corresponding to a statistical optics physical description.

5. Discussion of results

The most immediately evident result here is that, in the thin crystal limit, η_{12} and χ_{12} provide totally different predictions. Figure 2 shows the field- and intensity-based collection efficiencies versus the collection-mode waists, for fixed pump waist. When the collection waist is much greater than the pump waist, η_{12} asymptotically goes to 1, while χ_{12} goes to 0; in the opposite condition ($w_p \gg w_o$), $\eta_{12} \rightarrow \frac{1}{2}$ and $\chi_{12} \rightarrow 1$. However, the thin-crystal approximation is far from valid unless the crystal is shorter than 0.1 mm for these collection beam diameters. In practical

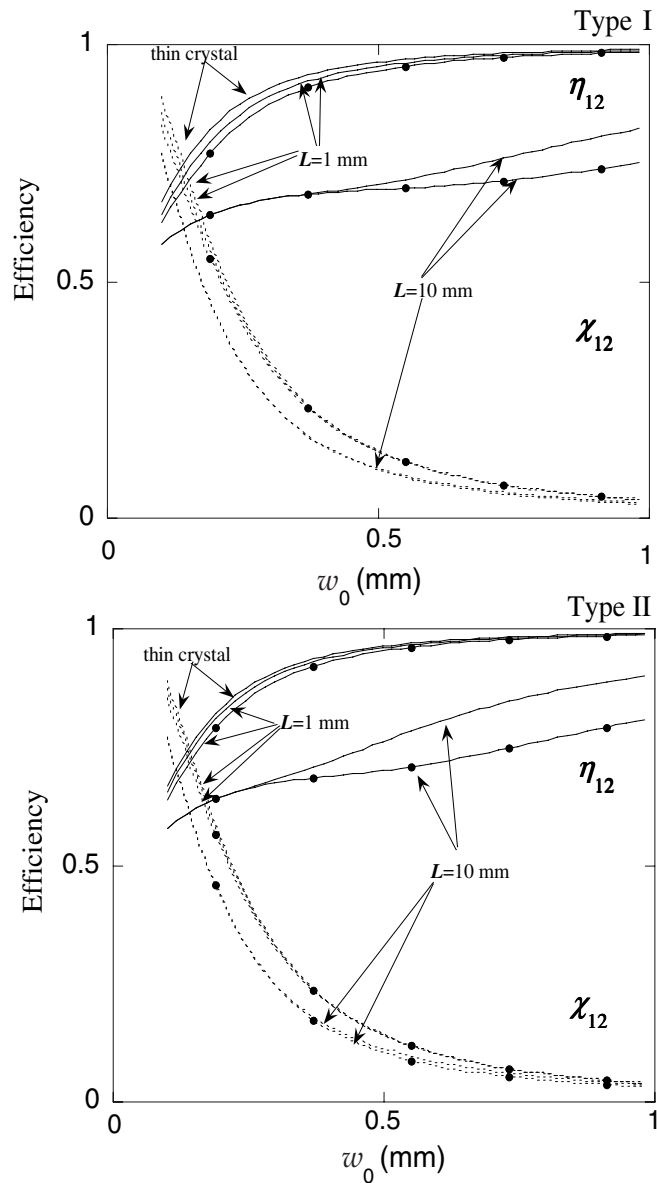


Figure 4. Plots of η_{12} (solid lines) and χ_{12} (dashed lines) versus w_o for fixed $w_p = 100 \mu\text{m}$ and $L = 1$ and 10 mm. We simulated the case of type I (upper panel) for collinear and non-collinear (with extra dots) conditions with $\gamma_p = 3.5^\circ$, $\mathcal{N}_p = -1.4 \mu\text{m}^{-1}$ and type II (lower panel) for collinear and non-collinear conditions (extra dots), $\mathcal{N}_p = -1.67 \mu\text{m}^{-1}$, and $\mathcal{N}_s = -0.77 \mu\text{m}^{-1}$.

cases, crystal length ranges from 0.5 to 20 mm. This is one of the prime motivations for this work.

To illustrate a practical lab setup, we consider a BBO crystal with type I and II phase-matching, pumped at 458 nm and look at downconversion at the degenerate wavelength (916 nm). For both type I and II, we describe the collinear and non-collinear cases with $\theta_s = \theta_i \cong 1.5^\circ$. To make valid predictions, we must ensure that the combination of L and w_p satisfy the assumptions

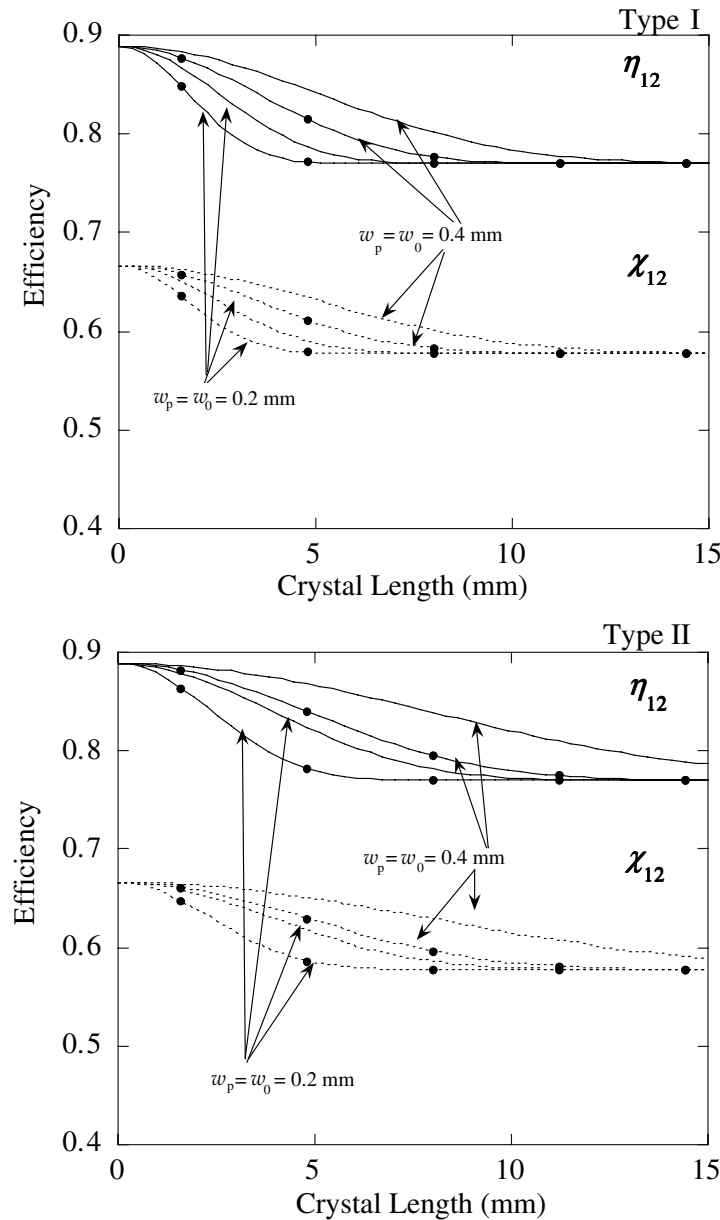


Figure 5. Plots of η_{12} (solid lines) and χ_{12} (dashed lines) versus L for fixed $w_p = w_o = 0.2$ mm and $w_p = w_o = 0.4$ mm. We simulated the cases of type I (upper panel) and type II (lower panel). Both non-collinear PDC output (as indicated by the curves with dots) and collinear PDC output (curves without dots) configurations were calculated with all other parameters the same as in the previous figure.

made in deriving the expression. Figure 3 shows a graph of valid parameter combinations generally putting a lower limit on the size of the pump waist.

Figure 4 plots both η_{12} and χ_{12} versus w_o for fixed $w_p = 0.1$ mm and crystal lengths of $L = 1$ and 10 mm, with their limit values referred to the thin crystal approximation. Cases of collinear and non-collinear configurations for both type I (figure 4 (upper panel)) and type II (figure 4

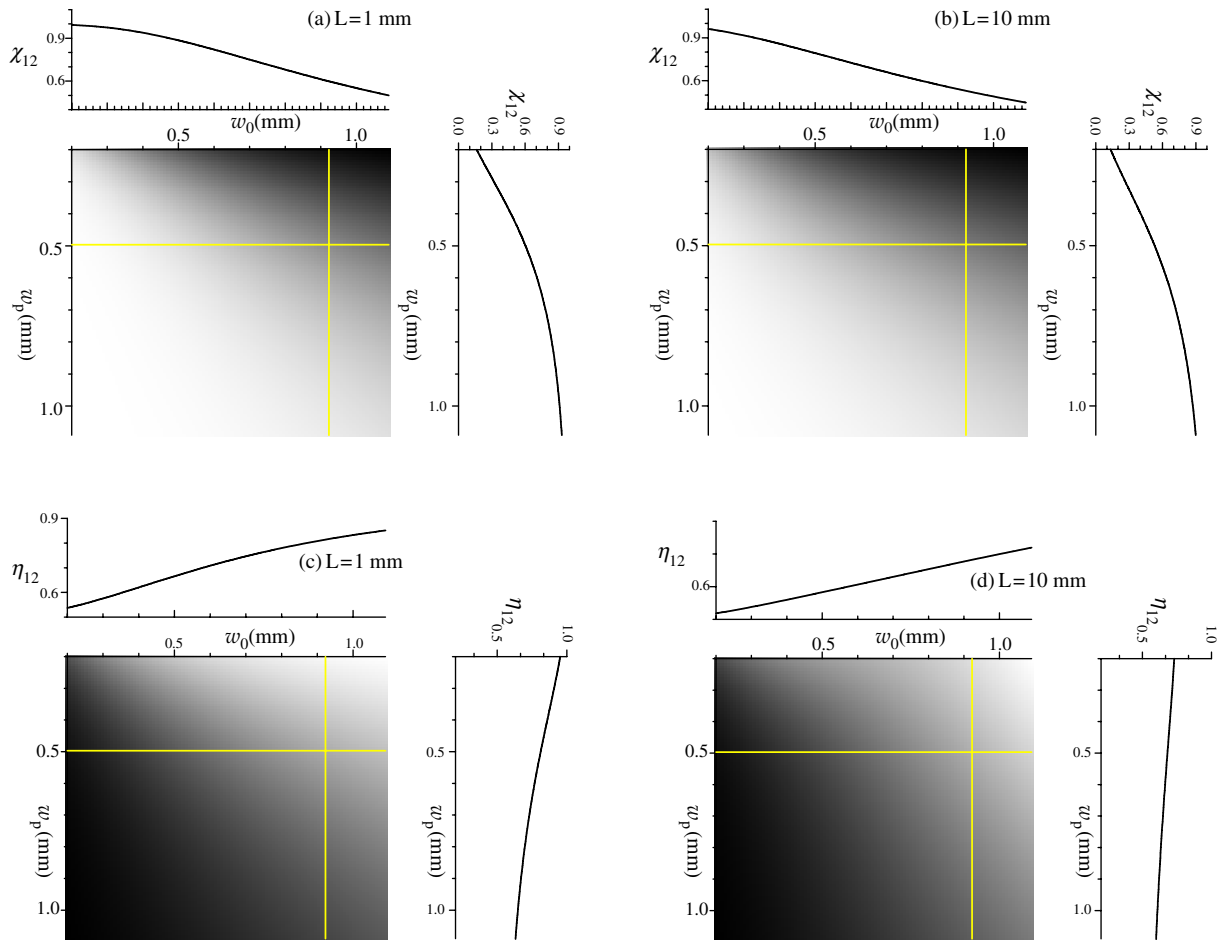


Figure 6. Density plots of χ_{12} (a,b) and η_{12} (c,d) versus w_o , w_p , for $L = 1$ mm (a,c) and 10 mm (b,d) respectively, in the case of type II non-collinear phase-matching. The lighter area corresponds to higher efficiency.

(lower panel)) phase-matching are plotted. Again, note the different behaviours of η_{12} and χ_{12} . When a crystal longer than 0.1 mm is used, both η_{12} and χ_{12} can be significantly reduced if the pump and collection waists are not properly matched. The way to match the waist for the optimum collection efficiency is different for η_{12} and χ_{12} . In particular, η_{12} can be optimized for a long crystal by increasing the collection waist at the crystal. The opposite holds for χ_{12} . Moreover, for η_{12} in the case of type I phase-matching (figure 4 (upper panel)), we observe that the collinear configuration always guarantees a better coupling, whereas this is not the case for type II. This can be observed for η_{12} evaluated at $L = 10$ mm in figure 4 (lower panel): for $w_0 < 0.5$ mm the non-collinear configuration appears clearly more efficient than the collinear one. We can justify this behaviour, because in type II collinear phase-matching the walk-off angle of the signal is less than that in the non-collinear configuration.

Figure 5 shows the effects of the crystal length on η_{12} and χ_{12} with $w_p = w_o = 0.2$ mm and $w_p = w_o = 0.4$ mm. We observe that, apart from their different values, η_{12} and χ_{12} present completely analogous dependences on the length of the crystal: all the chosen configurations (namely type I and II, collinear and non-collinear) converge to the thin crystal curve for very-short lengths. In

fact, for $L \rightarrow \infty$, the factor \mathcal{F} in (28) approaches 1, thus the long crystal asymptotic values can be obtained directly from (31) and (27).

In general, the coupling efficiencies are higher in type I than II, and collinear geometry yields the best coupling efficiencies. It is noteworthy to observe that the dependence on the crystal length is actually rescalable, by scaling the pump and collection waists.

Figure 6 plots χ_{12} and η_{12} versus w_o and w_p for two different lengths of the crystal.

Because of other effects that can lower the efficiency in practice (such as crystal and optical losses, detector inefficiencies, and so on [29]), it is important to make an experimental test of the theory that is not sensitive to these extraneous types of losses. With this view, it is best to choose a configuration where the two models have opposite dependences on adjustable experimental parameters. For example, one could measure the collection efficiency for fixed crystal lengths, while varying either the pump waist or the collection waist, such as in central value range of figure 4.

6. Conclusions

We have presented an analytical model to quantify the collection efficiency in terms of adjustable experimental parameters with the goal of optimizing single-mode collection from two-photon sources. In addition, we have presented an alternative scheme that may have more validity for multi-mode collection arrangements. Our calculation was performed using generally accepted approximations such as relying mainly on a finite transverse distribution of the fields involved and neglecting second-order terms in the transverse wavevector's components. These calculations cover a wide range of experimental configurations and yield two formulas to quantify the collection efficiencies. We have pointed out experimental conditions that could be used to differentiate between the two models.

Acknowledgments

This work was supported in part by DARPA/QUIST, ARDA, ARO and partially by Elsag SpA/Qcrypt.

References

- [1] Bennett C and Brassard G 1984 *Proc. IEEE Int. Conf. on Computers, Systems and Signal Processing* (Bangalore) p 175
- [2] Bennett C and Brassard G 1985 *IBM Tech. Disclosure Bull.* **28** 3153
- [3] Bennett C and Brassard G 1989 *SIGACT News* **20** 78
- [4] Bennett C H, Bessette F, Brassard G, Salvail L and Smolin J 1991 *Lecture Notes in Computer Science* **473** 253
- [5] Ekert A 1991 *Phys. Rev. Lett.* **67** 661
- [6] Bennett C 1992 *Phys. Rev. Lett.* **68** 3121
- [7] Bennett C H, Brassard G and Mermin N D 1992 *Phys. Rev. Lett.* **68** 557
- [8] Ekert A K, Rarity J G, Tapster P R and Palma G M 1992 *Phys. Rev. Lett.* **69** 1293
- [9] Tittel W, Brendel J, Zbinden H and Gisin N 2000 *Phys. Rev. Lett.* **84** 4737
- [10] Knill E, Laflamme R and Milburn G J 2001 *Nature* **409** 46

- [11] Brassard G, Lutkenhaus N, Mor T and Sanders B C 2000 *Phys. Rev. Lett.* **85** 1330
- [12] Jacobs B C and Franson J D 1996 *Opt. Lett.* **21** 1854
- [13] Kim J, Benson O, Kan H and Yamamoto Y 1999 *Nature* **397** 500
- [14] Kurtsiefer C, Mayer S, Zarda P and Weinfurter H 2000 *Phys. Rev. Lett.* **85** 290
- [15] Buttler W T, Hughes R J, Lamoreaux S K, Morgan J L, Nordholt J E and Peterson C G 2000 *Phys. Rev. Lett.* **84** 5652
- [16] Yaun Z, Kardynal B, Stevenson R, Shields A, Lobo C, Cooper K, Beattie N, Ritchie D and Pepper M 2001 *Science* **10.1126** 1066790
- [17] Pittman T B, Jacobs B C and Franson J D 2002 *Phys. Rev. A* **66** 042303
- [18] Beveratos A, Bruori R, Gacoin T, Villing A, Poizat J-P and Grangier P 2002 *Phys. Rev. Lett.* **89** 187901
- [19] Migdall A, Branning D and Castelletto S 2002 *Phys. Rev. A* **66** 053805
- [20] Migdall A L, Castelletto S, Degiovanni I P and Rastello M L 2002 *Appl. Opt.* **41** 2914
- [21] Monken C H, Ribeiro P H S and Padua S 1998 *Phys. Rev. A* **57** R2267
- [22] Kurtsiefer C, Oberparleiter M and Weinfurter H 2001 *Phys. Rev. A* **6402** 023802
- [23] Bovino F A, Varisco P, Colla A M, Castagnoli G, Di Giuseppe G and Sergienko A V 2003 *Opt. Commun.* **227** 343
- [24] Castelletto S, Degiovanni I P, Ware M and Migdall A L 2003 *Preprint* quant-ph/0311099
Castelletto S, Degiovanni I P, Ware M and Migdall A L 2003 *SPIE Proc.* 5161 (San Diego) p 48
- [25] Aichele T, Lvovsky A I and Schiller S 2002 *Eur. Phys. J. D* **18** 237
- [26] Rubin M H 1996 *Phys. Rev. A* **54** 5349
- [27] Ghatak A and Thyagarajan K 1998 *Introduction to Fiber Optics* (Cambridge: Cambridge University Press)
- [28] Klyskho D N 1988 *Phys. Lett. A* **132** 299
- [29] Castelletto S, Degiovanni I P and Rastello M L 2003 *Phys. Rev. A* **67** 022305